Biointerphases (2012) 7:29
DOI 10.1007/s13758-012-0029-7

ARTICLE

Surface Coating as a Key Parameter in Engineering Neuronal Network Structures In Vitro

Yi Sun · Zhuo Huang · Wenwen Liu · Kaixuan Yang · Kang Sun · Shige Xing · Dong Wang · Wei Zhang · Xingyu Jiang

Received: 30 December 2011 / Accepted: 2 April 2012 / Published online: 24 April 2012

Abstract By quantitatively comparing a variety of macromolecular surface coating agents, we discovered that surface coating strongly modulates the adhesion and morphogenesis of primary hippocampal neurons and serves as a switch of somata clustering and neurite fasciculation in vitro. The kinetics of neuronal adhesion on poly-lysine-coated surfaces is much faster than that on laminin and Matrigel-coated surfaces, and the distribution of adhesion is more homogenous on poly-lysine. Matrigel and laminin, on the other hand, facilitate neuritogenesis more than poly-lysine does. Eventually, on Matrigel-coated surfaces of self-assembled monolayers, neurons tend to undergo somata clustering and neurite fasciculation. By replacing coating proteins with cerebral astrocytes, and patterning neurons on astrocytes through self-assembled monolayers, microfluidics and micro-contact printing, we found that astrocyte promotes soma adhesion and astrocyte processes guide neurites. There, astrocytes could be a versatile substrate in engineering neuronal networks in vitro. Besides, quantitative measurements of cellular responses on various coatings would be valuable information for the neurobiology community in the choice of the most appropriate coating strategy.

Y. Sun and Z. Huang contributed equally to this work.

Electronic supplementary material The online version of this article (doi:10.1007/s13758-012-0029-7) contains supplementary material, which is available to authorized users.

Y. Sun · Z. Huang · W. Liu · K. Yang · K. Sun · S. Xing · D. Wang · W. Zhang (✉) · X. Jiang (✉)
CAS Key Lab for Biological Effects of Nanomaterials and Nanosafety, National Center for NanoScience and Technology, Beijing 100190, People's Republic of China
e-mail: zhangw@nanoctr.cn

X. Jiang
e-mail: xingyujiang@nanoctr.cn

Y. Sun · Z. Huang · W. Liu · K. Sun · S. Xing · D. Wang
Graduate School of the Chinese Academy of Sciences, Beijing 100864, People's Republic of China

1 Introduction

There is a growing interest in engineering neuronal networks in vitro [1, 2]. Such artificial neuronal networks have been employed as models for studying the functions of neuronal network [3–5] for engineering artificial intelligence [6, 7] and for neuro-interfacing [8]. As neurons are the building blocks of neuronal networks, technically, in order to construct a neuronal network, one has to control the positioning of the somata of the neuron, the guidance of the axons and the dendrites of neurons into specific locations and orientations. The realization of such designs, i.e., the engineering of the networks, requires delicate control of neuronal adhesion and morphogenesis.

Development in micro- nano- technology has brought in several new tools for engineering the patterning of cell adhesion and morphogenesis [9–13]. Many cell types have been successfully patterned with microfluidics [14–16], μCP [17], inkjet printing [18, 19], plasma treatment [20], self-assembled monolayers [21–24], self-assembled constructs [25], laser scanning lithography [26], atomic force microscope lithography, dip-pen nanolithography [27], topography [28, 29], carbon nano-tubes [30], or their combinations [31, 32]. Neurons are, however, distinctive cells with highly polarized morphology, much smaller somata, and thus few anchoring points for adhesion in comparison to most types of adherent mammalian cells. These features make the patterning of neurons especially

difficult. The development of polarized morphology follows cell adhesion, and continues for days and weeks before maturation, introducing additional challenges for engineering the neurites after the establishment of the patterns of adhesion. Microfluidics [33–36] has been used for positioning neuronal somata. However, culturing neurons within microfluidic chips over long terms is a challenge, possibly due to limited nutrient exchange. Surface chemistry [37–39] allowed elegantly patterned neuronal networks with potentially useful functions, but long term maintenance of the networks is a problem. SAMs [40, 41] represent a convenient way for engineering cell adhesion [42], as SAMs do not involve complicated instruments during the experiment. Coating is widely used for tailoring the biocompatibility of the neuron-materials interfaces [43–45]. Various coating agents have been used, but few studies systematically investigated the effectiveness of these molecules in adhesion and morphogenesis. We hereby set out to study how surface coating alone affects the adhesion, morphogenesis and therefore network structure of neurons, and building ordered neuronal networks with these coating strategies.

2 Experimental

2.1 Micro-Fabrication, Self-Assembled Monolayers and Microfluidics

Standard photolithography and soft lithography were employed for fabricating microfluidic channels and the stamps for micro-contact printing. AutoCAD (Autodesk) was used for designing the masks and high-resolution printer was employed afterwards for generating the masks. The master was fabricated through standard photolithography on a mask aligner (MJB4, Suss MicroTec) with SU-8 2025 and 2100 photo-resist (MicroChem). Poly-dimethylsiloxane (PDMS, Dow Corning) replica molding was performed to obtain the elastic stamps for micro-contact printing and the microfluidic channels.

Patterned SAMs was created according to standard protocol with thiols on gold plates. Gold plates were prepared by firstly evaporating a layer of 8 nm-thick titanium, followed by a 40 nm of gold, both with an vacuum electron-beam evaporator (Edward Auto 500), on acid-rinsed glass cover-slips. Alkanethiols terminated with $-CH_3$ ($HS(CH_2)_{15}CH_3$, Sigma) were used for creating patterns to promote cell adhesion through μCP. Patterned gold substrates were immersed in $-EG_6$ terminated thiols ($HS(CH_2)_{11}(OCH_2OCH_2)_3OH(C_{11}EG_3)$, Sigma) for 2 h at ambient temperature to make the rest of the surfaces antifouling.

2.2 Surface Coatings

We used Matrigel (MG, BD Biosciences, 1:100 v/v in serum free DMEM), laminin (LN, R&D Systems and BD Biosciences, 50 μg/mL in Dulbecco's phosphate buffer saline, D-PBS), fibronectin (FN, BD Biosciences, 25 and 50 μg/mL in D-PBS), polyethyleneimine (PEI, Sigma, 25 and 50 μg/mL in sterile water), poly-D-lysine (PDL, Sigma, molecular weight 70,000–150,000, 25 and 50 μg/mL in sterile water.), poly-L-lysine (PLL, Sigma, MW 70,000–150,000. 25 and 50 μg/mL in sterile water), as the coating layer over glass cover slips on which neurons were seeded. These are most frequently used coating agents for neuronal culture. The coating procedures were strictly consistent between different coating agents: all agents were applied for 2 h at 37 °C, rinsed with corresponding solutions (sterile water for polymers and D-PBS for proteins) and incubated with plating medium.

Patterned SAMs were coated with PLL, LN, and MG respectively, incubated for 2 h at 37 °C, then rinsed with D-PBS and incubated with DMEM/F12 medium supplemented with 10 % of horse serum at 37 °C before plating neurons.

To generate patterns like those in Fig. 8, PDMS stamps were treated with air plasma (Harrick Scientific), μCP of LN (200 μg/mL) stripes was performed directly on acid rinsed glass cover slips. PDMS microfluidic channels were sealed with the substrate, keeping the channels perpendicular to the laminin stripes. PLL (50 μg/mL) was used to promote cell adhesion in the channel areas [46]. The channel was incubated with DMEM/F12 medium supplemented with 10 % of horse serum at 37 °C. We introduced purified astrocytes into one of the channels with DMEM/F12 medium supplemented with 10 % of horse serum at 37 °C, and they adhered and spread before we introduced neurons into the other channel, also with DMEM/F12 medium supplemented with 10 % of horse serum at 37 °C.

2.3 Primary Culture of Hippocampal Neurons and the Purification of Cerebral Astrocytes

Neonatal (P0) and embryonic (E18) Sprague–Dawley (SD) rat pups were decapitated, treated in 0.25 % Trypsin (GIBCO) supplemented with DNase I (Sigma) for 15 min at 37 °C water bath, and triturated. Dissociated neurons were seeded onto surfaces in DMEM/F12 medium (GIBCO) supplemented by 10 % horse serum (GIBCO).

After cell adhesion, the surfaces were rinsed gently with D-PBS three times depending on the cell density, and replaced with Neurobasal medium supplemented with 2 % B27 and 1 % GlutaMax-1 (all from GIBCO) without antibiotics. The medium were replaced by half every

4 days. All animal experiments were approved by IACUC of National Center for Nanoscience and Technology.

Cerebral astrocytes were obtained from P0 SD rats according to standard protocol [47] with modifications. In brief, cerebral cortex was treated in 0.25 % Trypsin (GIBCO) for 15 min at 37 °C water bath, and triturated. Dissociated tissues were filtered with membranes having 50 μm-sized pores, seeded onto untreated plastic culture clusters (Corning, TC treated grade) in DMEM/F12 medium (GIBCO) supplemented by 10 % horse serum (GIBCO) for 50 min. The supernatant were plated onto culture clusters pretreated with PDL (10 μg/mL) in order to exclude fibroblasts and epithelial cells that adhere faster. After 24 h of cell adhesion, the cultures were rinsed with D-PBS for three times, and refilled by DMEM/F12 with 10 % horse serum. The cultures were shaken every day, and the medium were replaced completely every 4 days to prohibit oligodendrocyte and neuron growth. At 14 days in vitro (DIV) when the cells form a contact-inhibited monolayer, the culture clusters were shaken at 220 rpm, 37 °C for 12 h to get rid of most of the contaminating oligodendrocyte. After that, each well was rinsed with warmed D-PBS for three times. Very high purity astrocyte could be obtained with this method.

2.4 Immunocytochemistry

Cell cultures were rinsed with D-PBS (37 °C) then fixed in 4 % paraformaldehyde for 30 min, followed by permeabilization with 0.3 % Triton X-100 for 15 min at ambient temperature. After blocking with 10 % goat serum in D-PBS for 1 h, primary antibodies against Tuj1 (Sigma), Smi312 (Covance) and GFAP (Sigma) were applied, and incubated overnight at 4 °C, followed by rinsing in D-PBS for 5 times and visualization with Alexa Fluor 488, 555, 633 conjugated secondary antibodies (1:400, Invitrogen). Rhodamine or Alexa Fluor 488 labeled Phalloidin (1:40, Invitrogen) was used for labeling actin cytoskeleton. Hoechst 33342 was used for labeling the cell nucleus. Samples were sealed with the mounting medium Anti-fade Gold (Invitrogen). All reagents were purchased from Sigma unless otherwise noted.

2.5 Imaging

Phase contrast imaging was carried out on Leica AF6000 live cell imaging workstation. Fluorescence imaging was performed with Zeiss LSM 710 or Olympus FV1000 laser scanning confocal microscope and Leica DMI 6000B wide-field fluorescence microscope. For fluorescence imaging, the samples were prepared up-side-down for imaging on inverted microscopes to avoid fluorescence quenching caused by the gold thin-film substrates. Imaging was performed immediately after preparation.

We used specific time points optimized for specific measurement and analysis: 4 h for adhesion (Fig. 1), 6 h for distribution (Fig. 2), 12 h for morphology (Fig. 3), 24 h for further analysis of morphology (Fig. 4) and 3-11 DIV for patterning (Fig. 6). We have chosen these time points for the convenience of measurements since the morphology of the cells at longer time points would be complicated for global analysis such as adhesion and distribution.

2.6 Data Processing and Statistics

Image quantifications were performed in ImageJ (NIH) NeuronStudio (Computational Neurobiology and Imaging Center, Mount Sinai School of Medicine) and Image Pro Plus (Media Cybernetics). These include the numbers of neurons adhered onto a specific surface (Figs. 1, 7), the locations of the neurons (Fig. 2) and morphological characters of neurons (Figs. 3, 4, 5, 8).

Data analysis was done in Matlab (The MathWorks).

Statistical analysis was performed by R (The R Foundation for Statistical Computing) and Stata (StataCorp). For groups of two conditions, statistical tests were performed using two-tailed Student's t test or Mann–Whitney U test. For groups of three or more conditions, one-way parametric ANOVA or Kruskal–Wallis' ANOVA were used, followed by Tukey–Kramer's or Bonferroni's post hoc multiple comparisons tests. Descriptive statistics are presented as mean ± SEM. All error bars designate SEM.

2.7 Measurement of Neuronal Adhesion

Neurons were rinsed thoroughly with D-PBS for three times after 4 h of adhesion, and immunocytochemistry with neuronal marker Tuj1, astrocyte marker GFAP. Actin was labeled with Alexa Fluor 488 labeled Phalloidin and cell nucleus was counterstained with Hoechst 33342. Phase contrast and fluorescence images were collected simultaneously. Cells were counted in as adherent neurons only if they satisfy three conditions simultaneously. Firstly, cells should assume normal neuron morphology. Phase contrast images of the cells should not be too bright (possibly indicating non-adherent cells) or too dark (sometimes dead cells). The size and shape of the nucleus should be that of a normal neuron. Secondly, they should be Tuj1 positive and GFAP negative. Thirdly, actin should be significantly weaker than that of astrocytes or fibroblasts. Cell numbers and locations were measured semi-automatically with ImageJ and Image Pro Plus. Locations of the cells were determined by calculating the geometric center of the somata profile with ImageJ. The somata profile was obtained by manually drawing lines around the somata.

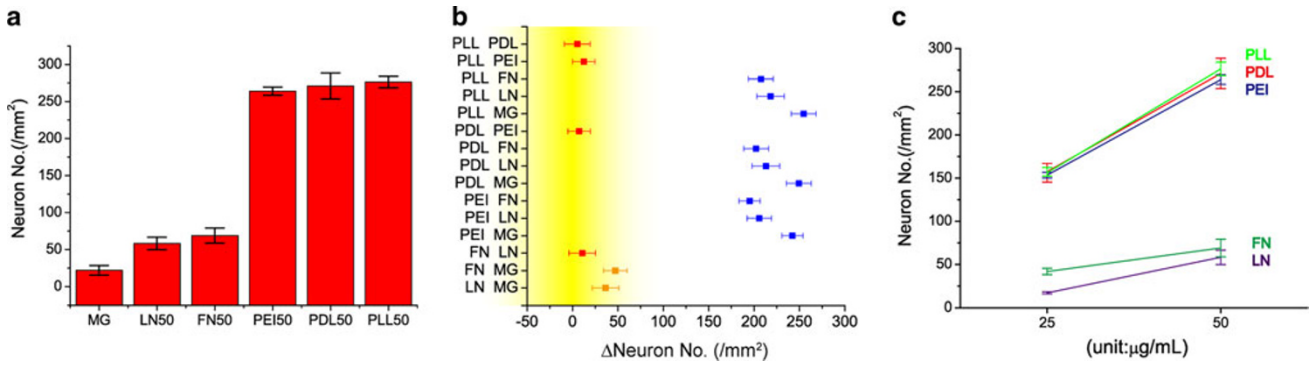

Fig. 1 Surface coating modulates the adhesion of neurons. **a** *Bar plot* showing the number of neurons adhered onto substrates with different coatings at 4 h after plating. The concentrations of the coating agents were 50 μg/mL except for MG, which was diluted to 1:100 v/v. MG: n = 6, LN: n = 4, FN: n = 6, PEI: n = 10, PDL: n = 5, PLL: n = 5. **b** Pair-wise comparisons between neuronal adhesion on different types of surfaces show that the number of neurons adhered onto different substrates are significantly different (Kruskal–Wallis ANOVA followed by Tukey–Kramer's post hoc multiple comparisons tests against the same dataset in **a**). *Red error bars* denote no significant difference, and this applies to FN against LN, and to any combination between PEI, PDL and PLL. *Yellow error bars* denote difference that are significant ($0.01 < P < 0.5$) depending on the standard chosen, and this applies to FN or LN against MG. *Blue error bars* denote significant difference ($P < 0.001$), and this applies to any combination between PEI, PDL or PLL against FN, LN or MG. *Yellow shaded* area highlights the significance zone. **c** The number of neurons adhered depends on the concentration of the coating agents (Students' *t* test, $P < 0.001$ for each pair, numbers of samples at 25 μg/mL, LN: n = 6, FN: n = 6, PEI: n = 10, PDL: n = 6, PLL: n = 5, numbers of samples at 50 μg/mL, same as those in **a**); *Error bars* SEM

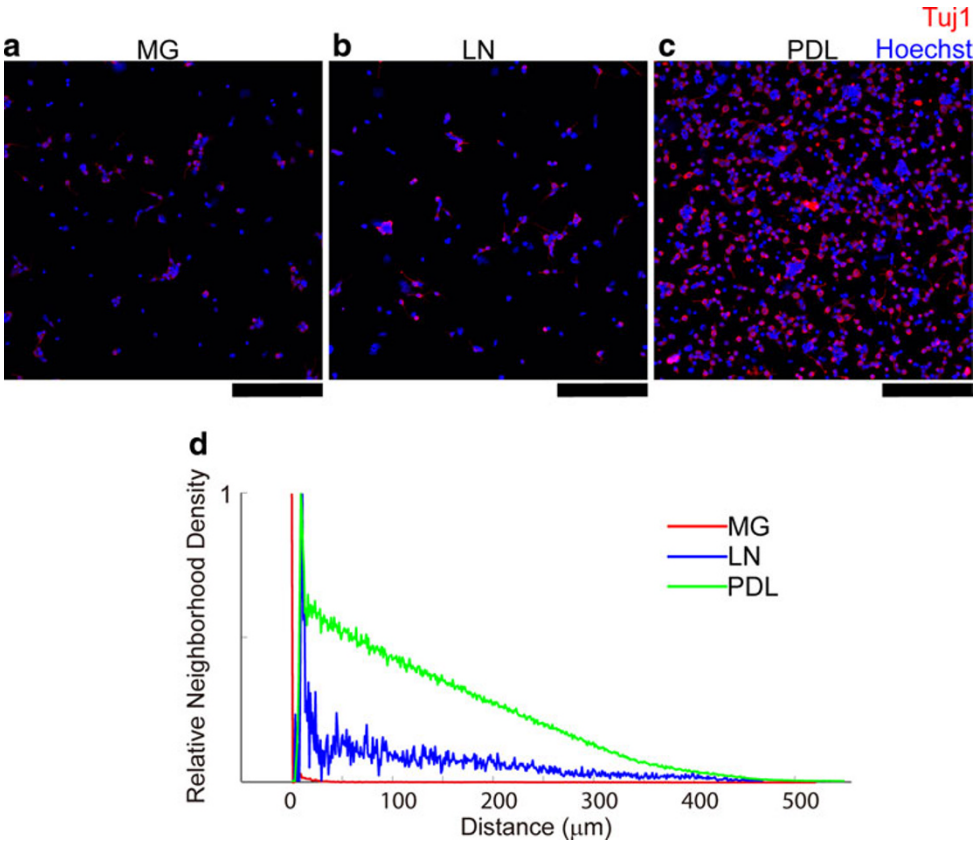

Fig. 2 Surface coating determines neuronal adhesion pattern. **a**–**c** Confocal fluorescence images of rat hippocampal neurons that were plated with the same density onto MG-, LN- and PDL-coated surfaces at 6 h after plating. Hoechst with *blue* pseudo-color labels the nucleus and *red* colored neuronal marker Tuj1 specifically labels neurons. **d** Normalized relative neighborhood density(see text for details) illustrating the extent of clustering on MG (*red*), LN (*blue*) and PDL (*green*) respectively. *Scale bar* 100 μm

The rate of neuronal adhesion was measured by time-lapse imaging. Coated substrates were monitored under live cell imaging workstation immediately after plating neurons. Neurons are considered to be adhered if they adhere and spread over the substrates and remain within focus for more than half an hour. We measured the time consumed by the adhesion process as the rate of adhesion.

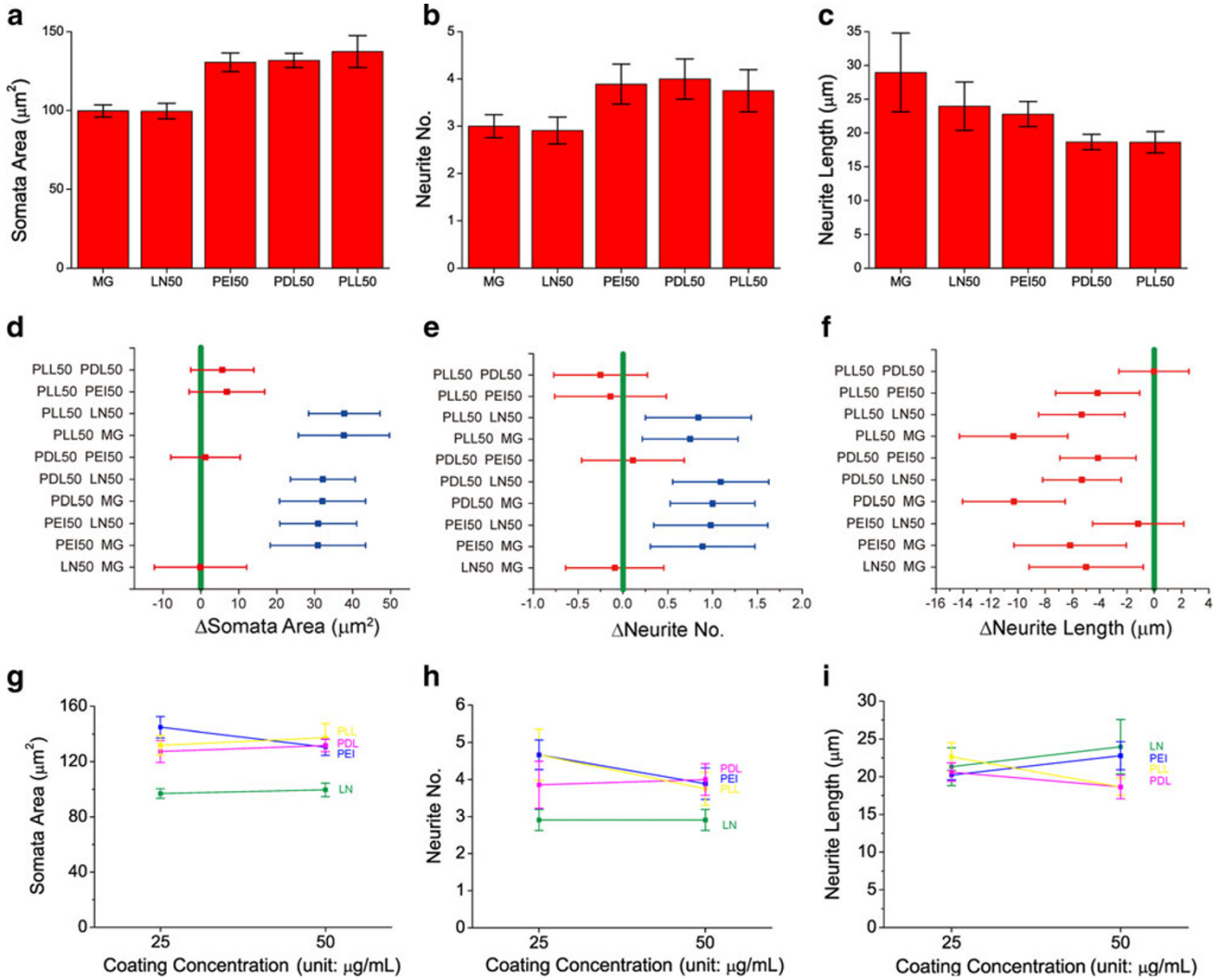

Fig. 3 Comparison of neuronal morphology on different surfaces at 12 h after plating. **a–c** *Bar plot* showing the somata area, neurite number and average neurite length of neurons on various surfaces (MG: n = 5, 5 data points; PEI 50 μg/mL: n = 5, 30 data points; PDL 50 μg/mL: n = 3, 76 data points; LN 50 μg/mL: n = 3, 32 data points; PLL 50 μg/mL: n = 3, 45 data points). **d–f** Multiple comparisons between different between different surface coating conditions corresponding to **a–c**. Somata areas and neurite numbers of neurons are significantly on various substrates ($P < 0.01$ for *blue error bars*, $P > 0.05$ for *red error bars*) while neurite lengths are not significantly different (Kruskal–Wallis ANOVA followed by Bonferroni's post hoc multiple comparisons tests). **g–i** Somata areas, neurite numbers and neurite lengths are not significantly different between surface coating agents at 25 and 50 μg/mL. (PEI 25 μg/mL: n = 5, 50 data points; PDL 25 μg/mL: n = 14, 60 data points; LN 25 μg/mL: n = 5, 15 data points; PLL 25 μg/mL: n = 9, 55 data points. Student's *t* test). *Error bars* SEM

2.8 Measurement of Neuronal Morphology

Phase contrast and fluorescence images were collected as above. Fluorescence images were used to as judgments of whether a structure is a neurite from a normal neuronal soma rather than debris. Measurements were performed with phase contrast images, as the signal is more consistent on fine distal part of neurites. The areas of the somata were measured by first draw splines around the somata and calculating the areas within the profile with ImageJ. The length and number of neurites were determined with models constructed in NeuronStudio. A neurite is confirmed if it is Tuj1 positive and bearing Phalloidin signal in the tips of the neurite. All neurites of a neuron is added together to obtain the neurite number. The longest neurite is determined by routines in Matlab.

2.9 Reconstruction of Neuronal Morphology and Sholl Analysis

Three-dimensional reconstruction of neuronal morphology (Fig. 5a–f) was performed with NeuronStudio.

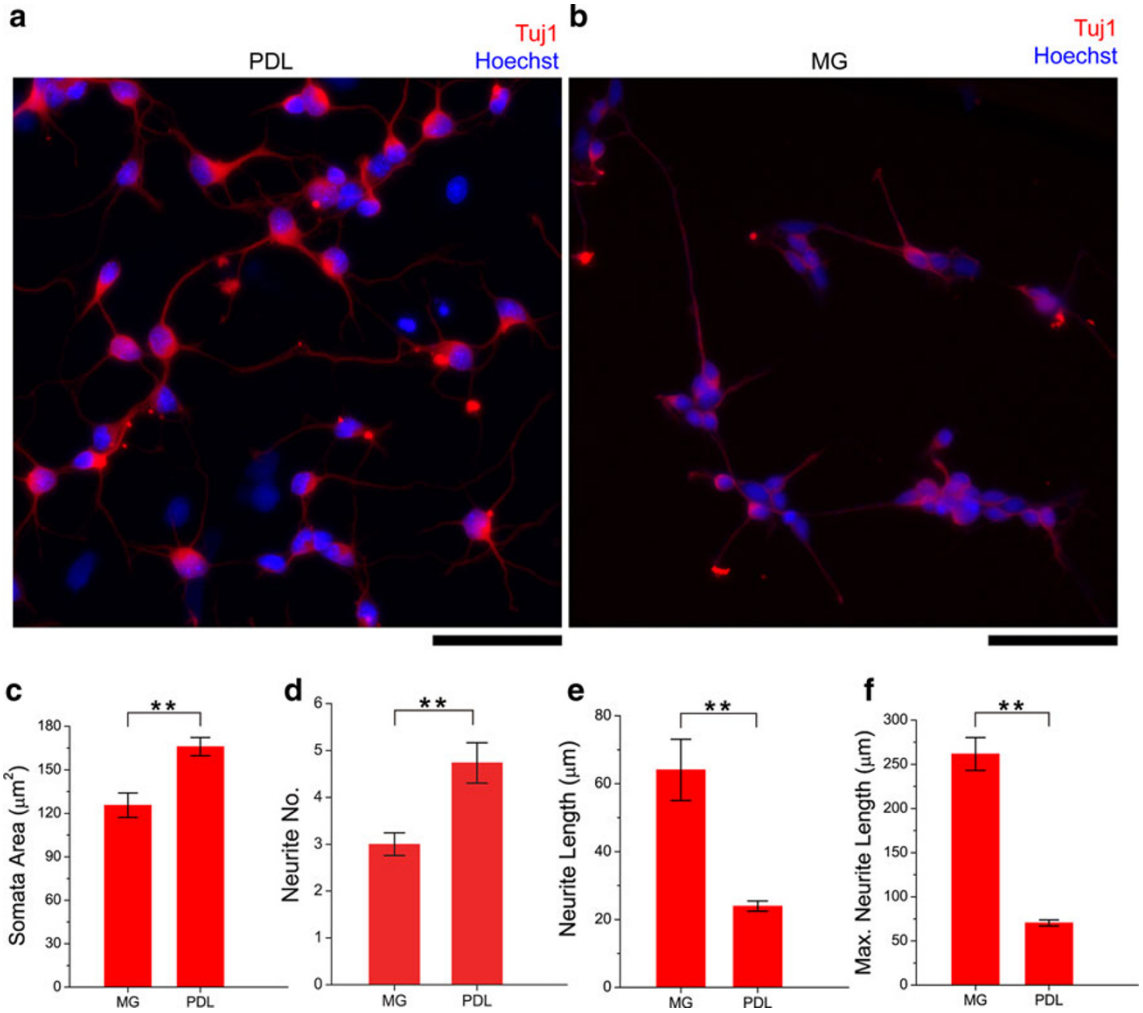

Fig. 4 Comparison of the morphology of neurons between PLL and MG at 24 h after plating. **a**–**b** Immunofluorescence photomicrographs of neurons on MG (**a**) and PDL (**b**) with neuron specific marker Tuj1, cell nuclei counterstained with Hoechst. Neurons on PDL surfaces develop more neurites, have shorter neurites, and the longest neurites are shorter compared to neurons on MG. See text for details. **c**–**f** Somata areas, neurite numbers, neurite lengths are the length of the longest neurite for each neuron are significantly different on MG and PDL (**c** MG, n = 5, PLL, n = 15; **d** MG, n = 17, PLL, n = 17; **e** MG, n = 11, PLL, n = 16; **f** MG, n = 5, PLL, n = 5. Mann–Whitney *U* test, **P < 0.01). *Scale bars* 200 μm

Sholl analysis (Fig. 5g, Supplementary Fig. 6) was performed with standard method via an ImageJ plugin (Ghosh Lab, UCSD).

Relative neighborhood density quantifies the neurons density with respect to the original position of a specific neuron, averaged for all neurons.

For a surface with N neurons, the distribution function of the neurons $n(r)$ is a variable that depends on the location of the plane, for arbitrary neuron i, we define its specific neighborhood density as:

$$D^i(r) = \frac{\sum_r n(r)}{\sum_r^{r+\delta} A(r)}$$

in which $A(r)$ is the area of an annuli with a distance of r from neuron i, with width δ.

We then have the relative neighborhood density by averaging over all N cells on the plane:

$$D(r) = \frac{\sum_{i=1}^{N} D^i(r)}{N}$$

In this paper, the width of the annuli δ, which defines the resolution of the analysis, is set to 1 μm.

2.10 Clustering Analysis

Clustering analysis was used for the quantitative classification of different types of molecules in terms of numbers of cells adhered and morphology. Euclidean distance was used for the measurement.

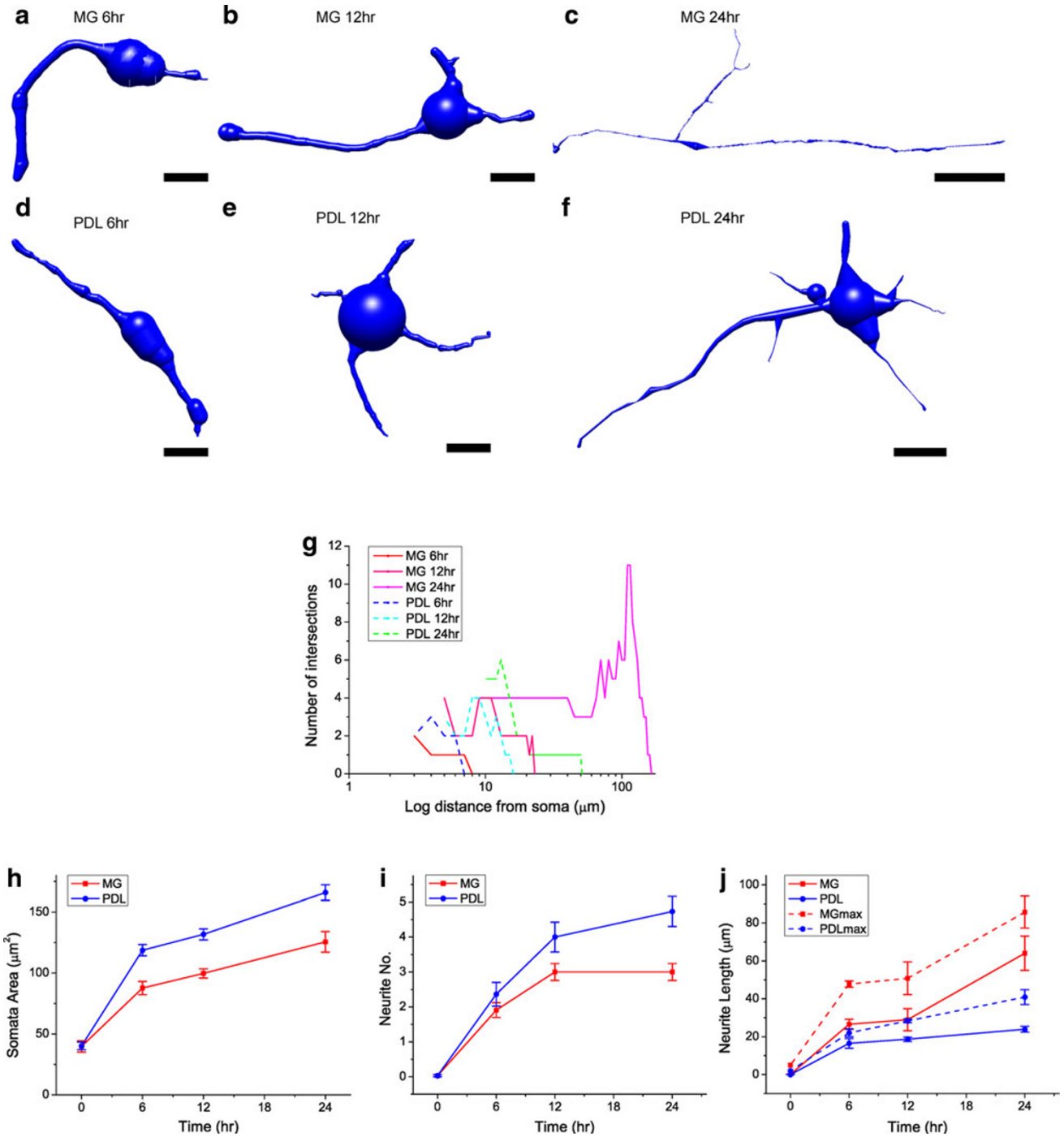

Fig. 5 Development of neuronal morphology on MG and PDL coated-surfaces within the first 24 h after plating. **a**–**f** Reconstruction of neuronal morphology on MG and PDL coated-surfaces at 6, 12 and 24 h after plating respectively. **g** Sholl analysis of typical neuron on MG and PDL coated-surfaces at 6, 12 and 24 h after plating respectively. See Supplementary Fig. 6 for details on the methods. **h**–**j** Time-dependent development of neuronal morphology on MG and PDL coated-surfaces in terms of somata area, neurite number and neurite length. In **j** MGmax and PDLmax designate the longest neurites. *Scale bars* **a** 5 μm, **b** 5 μm, **c** 50 μm, **d** 5 μm, **e** 5 μm, **f** 10 μm

3 Results and Discussion

3.1 Surface Coating Affects Neuron Adhesion

The number of neurons adhered onto coated glass surfaces depends significantly on the surface coatings at 4 h after plating (Fig. 1a). In generally, the numbers of cells on polymers (PEI: $264.00 \pm 5.52/mm^2$, $n = 10$; PDL: $271.20 \pm 17.51\ mm^2$, $n = 5$; PLL: $276.40 \pm 7.78/mm^2$, $n = 5$) is much higher than those on proteins (MG: $21.88 \pm 6.48/mm^2$, $n = 6$; LN: $58.25 \pm 8.33/mm^2$, $n = 5$; FN: $69.00 \pm 10.20/mm^2$, $n = 6$). There were significant differences between different coating agents at a given concentration (Fig. 1b, Kruskal–Wallis' ANOVA followed by Tukey–Kramer's post hoc multiple comparisons tests). There were significant differences between each combination of a protein with a polymer ($P < 0.001$, Fig. 1b). The numbers of cells adhered also depend significantly on the concentration of the coating agent ($P < 0.001$, Fig. 1c). We classified the coating agents according to the number of cells adhered using standard clustering analysis (Supplementary Fig. 1, see "Experimental" for details), and found that extracellular matrix (ECM) proteins (MG, LN and FN) are similar in terms of the amount of cells adhered while polymers (PEI, PDL, PLL) are also clustered. We found that a substantial portion of cells adhered onto FN coated surfaces are non-neuronal cells. We focused our discussions on MG, LN and PDL.

The distributions of adhesion are different between various surface coatings after 6 h of adhesion (Fig. 2). Neurons are homogeneously distributed on PLL-coated surfaces, but tend to cluster on LN- and MG- coated surfaces (Fig. 2a–c). As we will discuss later, the clustering process gradually occurred during the course of in vitro culture. In order to quantitatively measure the distribution of adhesion, we calculated the relative neighborhood density of the neurons (Fig. 2d). The relative neighborhood density [48] provides intuitive measurement of the probability for finding a neuron at a certain distance (see "Experimental" for details of the algorithm). The probability of finding another neuron on MG decays rapidly as the distance grows, indicating that neurons are highly clustered. Meanwhile, the curve decays much more slowly on PDL. We did another analysis by segmenting the photomicrographs into subunits with identical areas and enumerated the number of neurons present within each subunit (Supplementary Fig. 2). 3D column plots, which depict the number of neurons within each unit area, illustrate the highly heterogeneous distribution of neurons on MG and LN as compared with the case on PLL. The histogram, which shows the frequency at which a certain number of neurons fall within a unit, indicates that the adhesion process between PLL and MG are different random processes.

We measured the rate of adhesion on various substrates by time-lapse imaging (see "Experimental" for details). Neuronal adhesion is much faster on surfaces coated with polymers (2–5 min for PDL and PLL, $n = 5$. 5–10 min for PEI, $n = 5$) than on surfaces coated with polymers MG (1–3 h, $n = 3$), LN (2–4 h, $n = 3$) and FN (2–4 h, $n = 3$).

3.2 Surface Coating Regulates Neuron Morphogenesis

We quantified the morphologies of neurons on MG-, LN-, PEI-, PDL- and PLL- coated surfaces in terms of somata area, neurite number and neurite length at 12 h after plating (Fig. 3, see "Experimental" for details on measurements). This particular time window is chosen because morphological differences are evident at 12 h. Somata areas of neurons on various substrates were significantly different ($P < 0.01$, Kruskal–Wallis' ANOVA followed by Bonferroni's test, Fig. 3d), and there are significant differences between each combination of a protein with a polymer. The average area of soma on polymer-coated surfaces is $134.23 \pm 2.98\ \mu m^2$ ($n = 78$, data pooled from neurons on PDL, PLL and PEI). In contrast, neurons on MG- and LN-coated surfaces have an average area of about $102.43 \pm 6.80\ \mu m^2$ ($n = 25$). Neurons on protein coatings generally have 3 neurites at this time window, while those on polymers have 4 (Fig. 3b). The numbers of neurites assumed by each neuron on various coatings are significantly different ($P < 0.01$, Kruskal–Wallis' ANOVA followed by Bonferroni's test, Fig. 3e). The difference on the length of neurites is more elusive. While neurites on protein coatings are generally larger than those on polymers (Fig. 3c), there is no significance between them (Kruskal–Wallis' ANOVA, Fig. 3f). There is no significant difference of morphologies including somata area, neurite number and neurite length, among different polymeric coating agents at different concentrations (Student's t test, Fig. 3g–i). We classified the coating agents in terms of somata area, neurite number and neurite length using standard clustering analysis based on Euclidean distances (Supplementary Fig. 3), and found that extracellular matrix (ECM) proteins (MG, LN) are similar in terms of the amount of cells adhered while polymers (PEI, PDL, PLL) are also clustered in terms of somata area (Supplementary Fig. 3a) and neurite length (Supplementary Fig. 3b), but results is counterintuitive in terms of neurite number (Supplementary Fig. 3c).

As neurons within their categories (polymers or proteins) exhibit characteristic morphological features, we focus our discussion on PDL and MG and extended culture time into the time window of 24 h.

After 24 h of in vitro culture, neuronal morphology is significantly different between PDL and MG (Fig. 4a, b). The somata area of neurons on PDL surfaces are larger and appear dark under phase contrast microscopy (MG: 125.55 ± 8.42 μm^2, PDL: 165.98 ± 6.32 μm^2, $P < 0.01$, Mann–Whitney *U* test, Fig. 4c), indicating that they spread more and are thinner, and the distribution of their somata areas span across a fairly wide range (Supplementary Fig. 4). Besides, each neuron on PDL develops more neurites (MG: 3.00 ± 0.24, PDL: 4.73 ± 0.43, $P < 0.01$, Mann–Whitney *U* test, Fig. 4d). Neurons cultured on PDL have shorter processes than their MG counterparts (MG: 64.04 ± 9.02 μm, PDL: 23.95 ± 1.49 μm, $P < 0.01$, Mann–Whitney *U* test, Fig. 4e). In particular, the longest neurites on MG are several times longer than those on PDL after 24 h of in vitro culture (MG: 261.68 ± 18.66 μm, PDL: 70.33 ± 3.51 μm, $P < 0.01$, Mann–Whitney *U* test, Fig. 4f). Because the significantly longer neurites are presumably axons [49], this result indicates that MG may accelerate axon specification by promoting the growth of the longest neurite.

We further studied the development of neuronal morphology within the first 24 h after plating (Fig. 5). Morphology of neurons cultured on MG- and PDL- coated surfaces at 6, 12 and 24 h after plating were reconstructed (Fig. 5a–f). While neurons on PDL-coated surfaces feature more neurites than their MG counterparts, the neurites is significantly longer for neurons on MG-coated surfaces. This is clearly shown on the sholl analysis (Fig. 5g, see Supplementary Fig. 6) as the initial value of intersections for neurons on PDL-coated surfaces is always higher than those on MG-coated surfaces. We also found that the peaks of the curves, which corresponds to the occurrences of branches, gradually shift rightwards, indicating the neurite branches takes places further away from the soma as neuron develops. The area of the somata (Fig. 5h) and the number of neurites (Fig. 5i) for neurons on MG-coated surfaces is smaller than those on PDL-coated surfaces. However, the length of the neurites (Fig. 5j) is longer for neurons on MG-coated surfaces, particularly for the longest neurites (MGmax and PDLmax), which would potentially grow into the axon. All parameters (area of somata, neurites number and length) exhibit time-dependent increase.

3.3 Surface Coating Affects Network Structure on Self-Assembled Monolayers in Long-Term Culture

SAMs is a robust technology for engineering cell adhesion in vitro. We patterned neurons into geometric shapes with SAMs treated with different molecules discussed above over several weeks. Briefly, patterns promoting neuron adhesion were formed through μCP with thiols terminated with $–CH_3$ on gold substrates evaporated on glass cover slips. The gold substrates were immersed in $–EG_6$ terminated thiols to make the rest of the surfaces anti-fouling (see "Experimental" for detailed methods).

We found that PDL coating on SAMs strongly affects surface patterning in long-term culture, particularly on patterns with features smaller than 1,000 μm. While immediate patterning works well, cells would grow onto PEG surfaces that are supposed to be anti-fouling after several days.

In contrast, MG surfaces lend well to long-term culture of patterned neuronal networks (Fig. 6). We used a pattern of concentric rings here. Neuronal networks could be robustly maintained up to a month. We also found that cells gradually cluster over time in long-term culture. The emergence of rings of clustering is a time-dependent process, taking place sometime around 6 DIV (Fig. 6). The clusters are located along the midlines of the concentric rings, and are laterally connected to form rings of clusters. Clustering was also frequently reported by other groups using other patterning approaches [37].

Polymeric surface coatings such as PDL cannot be used with the most robust technology, SAMs, to confine neurons into micro-patterns. While ECM protein coatings constitute a physically defined interface that affects neuronal adhesion and development, it would be interesting to see if other natural interfaces such as cell surfaces would affect neuronal patterning and development.

3.4 Astrocyte as Substrates for Engineering Neuronal Network Structure

Astrocytes are natural neighbors of neurons. There is accumulating evidence that astrocyte is a functionally indispensable part of neural circuits [50]. Banker and coworkers successfully evolved a method for co-culturing neurons with astrocytes for improving the viability of neurons [51]. In addition, the viability of astrocytes is more robust in culture, making it more straightforward to pattern astrocytes. We wondered if patterned cellular surfaces of astrocytes could be used in place of coating agents in experiments where patterning is necessary.

We introduced astrocytes onto SAMs of defined patterns treated with FN to form a patterned astrocyte monolayer (Fig. 7a), and plated neurons onto this layer (Fig. 7b). The kinetics and efficiency of neuronal adhesion on astrocytes falls between PLL and MG. Neurons adhere well over astrocytes, and after a few days in culture, neurons do not cluster on astrocytes severely (Fig. 7c). We studied the adhesion of neurons over patterned astrocytes plated at two densities (Fig. 7d). The numbers of adhered neurons over high-density astrocytes is 824.73 ± 37.51/mm^2 ($n = 8$) and over low-density astrocytes is 482.20 ± 17.90/mm^2 ($n = 10$). There are significant differences between the number of neurons adhered onto patterned astrocytes, MG

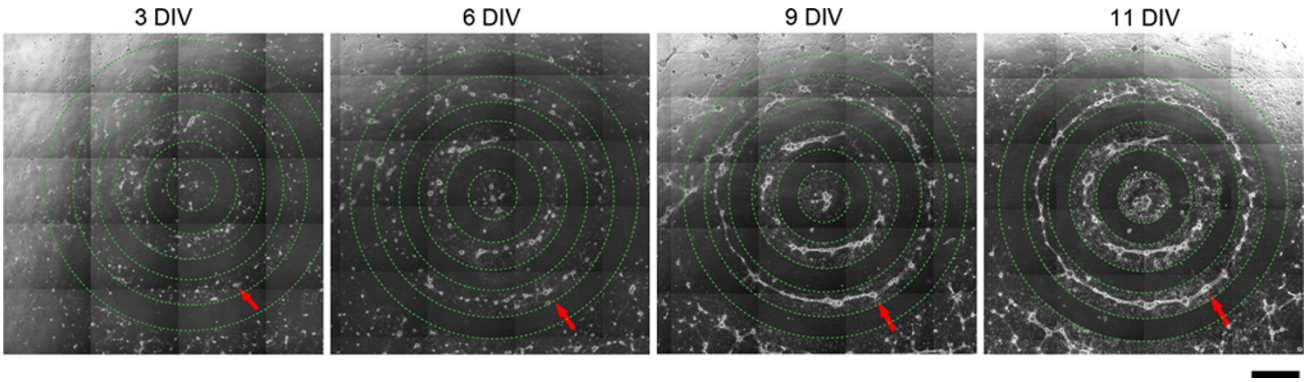

Fig. 6 Robust long-term culture of neuronal networks on MG-coated surfaces with geometric patterns. Time-lapse phase contrast imaging of concentric patterns after 3 days in vitro (DIV), 6 DIV, 9 DIV, 11 DIV, respectively. The *green dashed lines* highlight the edges of the pattern here and below. Clustering appears as early as at 6 DIV, and become strengthened with the passing of time (*red arrow*). *Scale bar* 100 μm, applicable for all four panels

and PDL coatings ($P < 0.001$, Kruskal–Wallis' ANOVA with Tukey–Kramer's post hoc test. $n = 8$ in high-density astrocyte pattern, $n = 10$ in low-density astrocyte pattern, $n = 9$ in PDL, $n = 6$ in MG, Fig. 7e). The difference between astrocytes at different densities is also significant ($P < 0.001$, Kruskal–Wallis' ANOVA with Tukey–Kramer's post hoc test. $n = 8$ in high-density astrocyte pattern, $n = 10$ in low-density astrocyte pattern, Fig. 7e).

We further studied how astrocytes could affect the polarized morphology of neurons. While there is a number of ways for patterning multiple types of cells controllably on the same substrate [52, 53], the specific morphology of neural cells that evolve polarized morphology after adhesion makes it essential to develop new methods for culturing multiple neural cells together. Through the combination of μCP with microfluidic channels (Fig. 8a), we found that astrocyte processes could be patterned with ordered orientation (Fig. 8b, red indicates astrocyte processes). These astrocyte processes could guide the extension of axons (Fig. 8b, green indicates axons, white arrows show where they are adjacent to each other). Three-dimensional reconstruction of the engineered neuronal network shows that neurites reside on or beside astrocyte processes (Fig. 8c). The compass plot shows orientation of neurites from neurons adjacent to astrocyte processes (Fig. 8d). Most of the neurites goes along the astrocyte processes (red, 0°, $n = 28$) or along the channel edges (blue, 90°, 270°, $n = 17$). The length of neurites guided by the astrocytes (236.00 ± 18.91 μm, $n = 10$) is significantly longer ($P < 0.001$) than those growing along the channel (70.20 ± 29.30 μm, $n = 10$, Fig. 8e).

4 Discussions

The assembly of neuronal circuit is a highly complicated dynamic process, in which neurites would grow and connect with each other, forming circuits. The number of cells adhered would affect the density and scale of the network. The relative position of the neurons (i.e., the spatial distribution of the somata) would affect the time required for neurites from these neurons to contact and connect with each other. The length of the neurites actually represents the temporal dynamics of neurite growth, and therefore affecting the connections between neurites. The number of neurites from each neuron would affect the complexity of the circuit. Altogether, the differences in adhesion and morphology are key parameters that control the spatiotemporal dynamics of circuit assembly and finally network structure, and the network structure substrates network function.

We found that surface coating strongly modulate the adhesion and morphology of the neurons. We systematic compared the abilities of regularly used coating agents as well as astrocytes in promoting neuronal adhesion. Polymeric coatings [54] such as PDL, PLL and PEI exhibit similar properties in adhesion and morphogenesis, while ECM proteins like MG and LN are similar to each other, and there are significant differences between polymeric coatings and extracellular proteins (Figs. 1, 2, 3, 4). Similar observations have been made on neuronal migration [55].

The number of neurons adhered are significantly higher on polymeric surfaces (Fig. 1a, b), indicating that the density of the network would be higher for polymeric surfaces. We also found the concentration of the coating agents to be an effective measure for controlling the number of adhered neurons (Fig. 1c).

Matrigel leads to somata clustering (Fig. 2a) and the process will get reinforced on SAMs (Fig. 6). On the contrary, the distribution of neurons is fairly homogenous over polymeric surfaces such as PDL (Fig. 2c, d). The distribution of neuronal somata will affect the formation of synaptic connections between neurons through contact of neurites after extensive development of the neurites, as adjacent

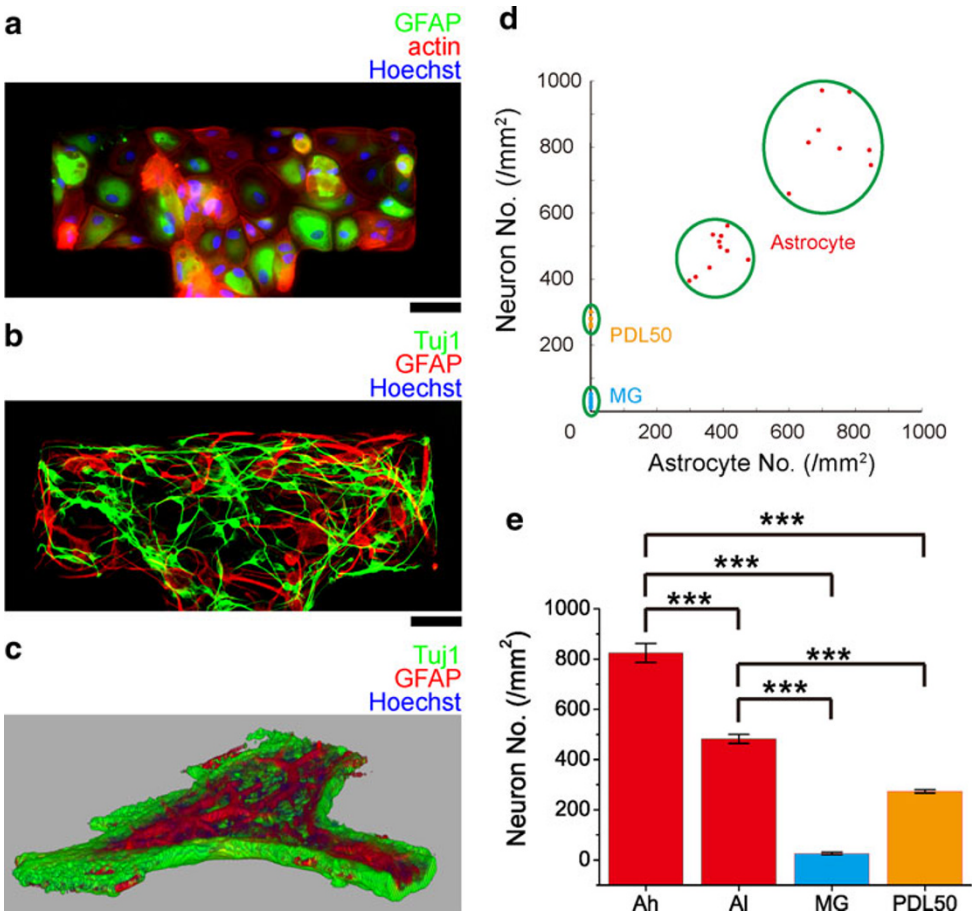

Fig. 7 Patterning neuronal networks via patterned astrocytes **a** Purified cerebral astrocytes patterned on SAMs. GFAP (*green channel*) is the astrocyte marker. This photomicrograph was taken 2 h after plating astrocytes. **b** Patterning neurons over patterned astrocytes. Neuronal marker Tuj1 and astrocyte marker GFAP are used to distinguish the two cell populations that are homogeneously distributed over the pattern. This laser scanning confocal photomicrograph was taken 1 DIV after plating neurons. **c** Three-dimensional reconstruction of the neuronal networks, the neuronal networks have developed extensively to envelop the astrocytes. Note that this picture is shown upside down. This laser scanning confocal photomicrograph was taken 6 DIV after plating neurons. **d** Scatterograph of the number of neurons per unit area with respect to the number of astrocytes underneath (if applicable). *Red dots* show the group in which neurons are seeded over astrocytes- patterned surfaces. This is further classified into two groups with astrocytes seeded at intentionally different densities. *Brown dots* show the group of 50 μg/mL PDL treated surface, and *blue dots* show the group of MG- treated surface. The data on PDL and MG for generating the figure here is the same set of data for Fig. 1. **e** Significance differences exist between astrocyte patterned surfaces and MG- and PDL- treated surfaces. Neuronal adherence is also significantly different on surfaces with different astrocyte density. Ah denotes high-density astrocyte pattern, Al denotes low-density astrocyte pattern. (***$P < 0.001$, Kruskal–Wallis's ANOVA with Tukey–Kramer's post hoc test. $n = 8$ in high-density astrocyte pattern, $n = 10$ in low-density astrocyte pattern, $n = 9$ in PDL, $n = 6$ in MG.) *Scale bars* 50 μm

neurons are more likely to be wired together. The uneven distribution of the somata therefore would lead to patches of more closely coupled sub-networks within a large network, the functional implication of which remains to be explored.

The larger soma areas on polymeric coatings (Figs. 3a, d, 4c) indicates that cells adhere more strongly over these surfaces. Neurons on polymeric surfaces exhibit much higher rate of adhesion, which is a further proof that the adhesion is stronger over these surfaces. Neurons also develop more neurites on polymeric coatings (Figs. 3b, e, 4d), and as a result, neurons on polymeric surfaces would have more exuberant arborizations, and the networks would be more complicated. ECM proteins such as Matrigel promote the growth of the neurites (Figs. 3c, f, 4e) and accelerate the establishment of neuronal polarity (Fig. 4f). As physiological characters of neurons are closely associated with neuronal morphology [56–58], the differences in morphological characters of neurons induced by different surface coatings would profoundly alter the function of the networks.

The observation that PDL negatively affects patterning in long-term culture reveals a potential drawback of polymeric coatings that was previously unexplored. While there are reports on the patterning of poly-lysine over PEG

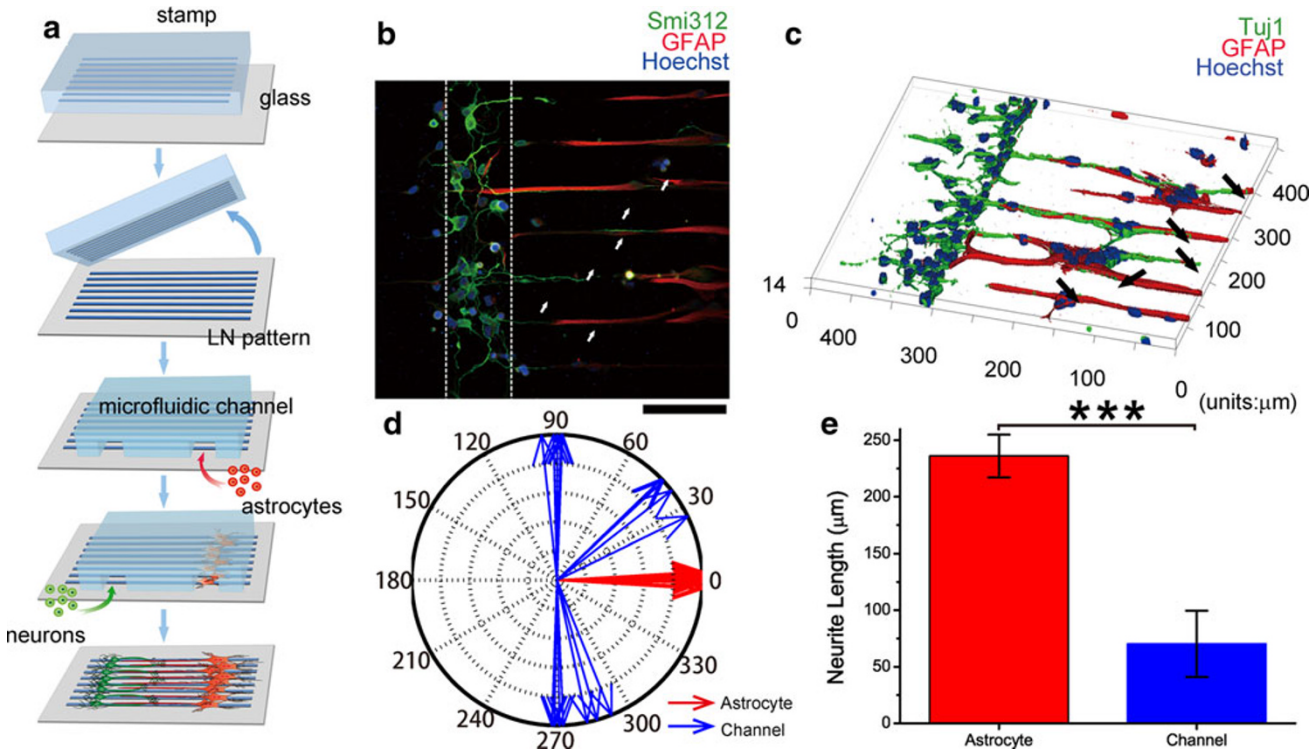

Fig. 8 Astrocyte-mediated patterning of neuronal networks. **a** Schematic illustration of the combination of micro-contact printing and microfluidics for patterning neurons and astrocytes together. **b** Immunocytochemistry showing that neuronal axons labeled by Smi312 (*green*) are guided by astrocytes GFAP (*red*). Astrocytes were patterned to extend long and slender processes in the horizontal direction. *White arrows* show where neuronal axons and astrocyte processes are adjacent to each other. **c** 3D confocal reconstruction of the neuronal networks formed by co-culturing neurons and astrocytes. Neurons are labeled with pan neuronal marker Tuj1, while astrocytes are labeled with GFAP. *Black arrows* show where neuronal processes and astrocyte processes are adjacent to each other. **d** The compass plot shows orientation of neurites from neurons adjacent to astrocyte processes. Most of the neurites go along the astrocyte processes (*red* 0°, n = 28) or along the channel edges (*blue* 90°, 270°, n = 17). **e** The length of neurites guided by the astrocytes is significantly longer than those growing along the channel (***$P < 0.001$, astrocyte: n = 28, channel: n = 17, Student's *t* test). *Scale bar* 200 μm. Units in **c** is μm

surfaces, our observation indicates that the long term robustness of anti-fouling effects of MG is better.

We found the modulation of adhesion and morphogenesis through surface coating to be robust, and these results could be tailored for specific experimental needs for engineering neuronal network structures.

Our study further shows that adhesion over astrocytes is the best (Fig. 8). As LN and MG exhibit largely similar property in terms of the numbers of neurons adhered, and taking into account that MG is a cocktail of ECM proteins including LN, LN is likely to be the key component in ECM for neuron adhesion [59]. The results seem to indicate that surface proteins on astrocytes contribute to the strong adhesion of neurons.

While the discussions here mainly evolved around SAMs and microfluidics, the data obtained here shed light on characteristics of neuronal adhesion and morphogenesis in other culture methods.

The discovery that astrocytes could be used for patterning neuronal adhesion and guiding neurites provides a new substrate onto which to engineer neuronal networks in vitro (Figs. 6, 7). While astrocytes were traditionally used for nurturing neuronal culture [51], we demonstrated the possibility to directly pattern neuronal adhesion and morphogenesis on astrocytes. As it is widely accepted that astrocytes are functionally indispensable parts of neural microcircuits, the capability to precisely engineer neurons and astrocytes simultaneously gives unprecedented access to study the interaction between neurons and astrocytes. While the method of using poly-lysine for coating and astrocytes for nurturing lends well to morphological studies of neuronal development, neuronal culture without astrocytes suffers from poor synaptogenesis [60], thereby preventing functional study of these networks. Our method of using astrocyte surfaces holds promise for building functional networks while making patterning possible.

Highly polarized morphology unique to neurons brings about a special challenge for patterning neuronal networks: there is actually infinite possibility of connectivity with the same pattern of somata location. However, only a few

patterns of connectivity potentiate functions. Engineering neuronal networks, therefore, requires engineering neurite guidance in addition to somata positioning. Our finding that astrocyte processes guides neurite processes as well as somata positioning point out a new paradigm for engineering neurite guidance and therefore network connectivity.

5 Summary and Conclusions

We quantitatively compared the adhesion and morphogenesis of several coating agents for neuron culture, and found significant differences between polymeric coatings and ECM proteins. We found surface coating to be a key parameter in modulating the adhesion and morphology of the neurons, both are important for circuit assembly hence network structure. We demonstrated in this paper the versatile capability of astrocytes, in combination with patterning methods through microfluidics and micro-contact printing, in positioning somata and guiding neurites that are essential steps towards engineered neuronal networks. We successfully constructed a neuronal network by patterning astrocytes first. By precise control of the surface coatings, various neuronal networks could be designed. These networks would be useful in applications ranging from basic neurobiology studies to neural prosthetic devices and artificial intelligence.

Acknowledgments We thank Yuan Dong for assistance with the experiments, Dingbin Liu, Drs. Yunyan Xie and Wenfu Zheng for helpful discussions, Drs. Zhuo Wang and Jiashu Sun for reading the manuscript, Dr. Xiang Yu of the Institute of Neuroscience, Chinese Academy of Sciences for critical comments. This study was supported by the Ministry of Science and Technology (2009CB930001, 2011CB933201, 2012AA030608), the National Science Foundation of China (51073045, 21025520, 90813032, 20890023), and the Chinese Academy of Sciences (KJCX2-YW-M15).

References

1. Silva GA (2006) Nat Rev Neurosci 7:65
2. Kotov NA, Winter JO, Clements IP, Jan E, Timko BP, Campidelli S, Pathak S, Mazzatenta A, Lieber CM, Prato M, Bellamkonda RV, Silva GA, Kam NWS, Patolsky F, Ballerini L (2009) Adv Mater 21:3970
3. Lau PM, Bi GQ (2005) Proc Natl Acad Sci USA 102:10333
4. Wilson NR, Ty MT, Ingber DE, Sur M, Liu G (2007) J Neurosci 27:13581
5. Segev R, Benveniste M, Hulata E, Cohen N, Palevski A, Kapon E, Shapira Y, Ben-Jacob E (2002) Phys Rev Lett 88:118102
6. Feinerman O, Rotem A, Moses E (2008) Nat Phys 4:967
7. Baruchi I, Ben-Jacob E (2007) Phys Rev E 75:050901
8. Straub B, Meyer E, Fromherz P (2001) Nat Biotechnol 19:121
9. Hu H, Ni YC, Montana V, Haddon RC, Parpura V (2004) Nano Lett 4:507
10. Whitesides GM, Ostuni E, Takayama S, Jiang XY, Ingber DE (2001) Annu Rev Biomed Eng 3:335
11. Dertinger SKW, Jiang XY, Li ZY, Murthy VN, Whitesides GM (2002) Proc Nat Acad Sci USA 99:12542
12. Sun Y, Liu YY, Qu WS, Jiang XY (2009) Anal Chim Acta 650:98
13. Khademhosseini A, Vacanti JP, Langer R (2009) Sci Am 300:64
14. Wang JY, Ren L, Li L, Liu WM, Zhou J, Yu WH, Tong DW, Chen SL (2009) Lab Chip 9:644
15. Chiu DT, Jeon NL, Huang S, Kane RS, Wargo CJ, Choi IS, Ingber DE, Whitesides GM (2000) Proc Nat Acad Sci USA 97:2408
16. Dworak BJ, Wheeler BC (2009) Lab Chip 9:404
17. James CD, Davis R, Meyer M, Turner A, Turner S, Withers G, Kam L, Banker G, Craighead H, Isaacson M, Turner J, Shain W (2000) IEEE Trans Biomed Eng 47:17
18. Roth EA, Xu T, Das M, Gregory C, Hickman JJ, Boland T (2004) Biomaterials 25:3707
19. Macis E, Tedesco M, Massobrio P, Ralteri R, Martinoia S (2007) J Neurosci Methods 161:88
20. Chang WC, Sretavan DW (2008) Langmuir 24:13048
21. Jans K, Van Meerbergen B, Reekmans G, Bonroy K, Annaert W, Maes G, Engelborghs Y, Borghs G, Bartic C (2009) Langmuir 25:4564
22. Ruiz A, Buzanska L, Gilliland D, Rauscher H, Sirghi L, Sobanski T, Zychowicz M, Ceriotti L, Bretagnol F, Coecke S, Colpo P, Rossi F (2008) Biomaterials 29:4766
23. Palyvoda O, Bordenyuk AN, Yatawara AK, McCullen E, Chen CC, Benderskii AV, Auner GW (2008) Langmuir 24:4097
24. Slaughter GE, Bieberich E, Wnek GE, Wynne KJ, Guiseppi-Elei A (2004) Langmuir 20:7189
25. Du YA, Lo E, Ali S, Khademhosseini A (2008) Proc Nat Acad Sci USA 105:9522
26. Hahn MS, Miller JS, West JL (2005) Adv Mater 17:2939
27. Piner RD, Zhu J, Xu F, Hong SH, Mirkin CA (1999) Science 283:661
28. Qiu C, Chen M, Yan H, Wu HK (2007) Adv Mater 19:1603
29. Liu Y, Sun Y, Yan H, Liu X, Zhang W, Wang Z, Jiang X (2011) Small 8:676
30. Dionigi C, Bianchi M, D'Angelo P, Chelli B, Greco P, Shehu A, Tonazzini I, Lazar AN, Biscarini F (2010) J Mater Chem 20:2213
31. Zhang J, Venkataramani S, Xu H, Song YK, Song HK, Palmore GT, Fallon J, Nurmikko AV (2006) Biomaterials 27:5734
32. Bai HJ, Shao ML, Gou HL, Xu JJ, Chen HY (2009) Langmuir 25:10402
33. Taylor AM, Rhee SW, Tu CH, Cribbs DH, Cotman CW, Jeon NL (2003) Langmuir 19:1551
34. Taylor AM, Dieterich DC, Ito HT, Kim SA, Schuman EM (2010) Neuron 66:57
35. Taylor AM, Blurton-Jones M, Rhee SW, Cribbs DH, Cotman CW, Jeon NL (2005) Nat Methods 2:599
36. Mahoney MJ, Chen RR, Tan J, Saltzman WM (2005) Biomaterials 26:771
37. Kleinfeld D, Kahler KH, Hockberger PE (1988) J Neurosci 8:4098
38. Stenger DA, Georger JH, Dulcey CS, Hickman JJ, Rudolph AS, Nielsen TB, Mccort SM, Calvert JM (1992) J Am Chem Soc 114:8435
39. Reska A, Gasteier P, Schulte P, Moeller M, Offenhausser A, Groll J (2008) Adv Mater 20:2751
40. Bain CD, Whitesides GM (1988) Science 240:62

41. Nuzzo RG, Allara DL (1983) J Am Chem Soc 105:4481
42. Wang H, He Y, Ratner BD, Jiang SY (2006) J Biomed Mater Res Part A 77A:672
43. Place ES, Evans ND, Stevens MM (2009) Nat Mater 8:457
44. Vogt AK, Wrobel G, Meyer W, Knoll W, Offenhausser A (2005) Biomaterials 26:2549
45. Heller DA, Garga V, Kelleher KJ, Lee TC, Mahbubani S, Sigworth LA, Lee TR, Rea MA (2005) Biomaterials 26:883
46. Delamarche E, Bernard A, Schmid H, Michel B, Biebuyck H (1997) Science 276:779
47. Mccarthy KD, Devellis J (1980) J Cell Biol 85:890
48. Condit R, Ashton PS, Baker P, Bunyavejchewin S, Gunatilleke S, Gunatilleke N, Hubbell SP, Foster RB, Itoh A, LaFrankie JV, Lee HS, Losos E, Manokaran N, Sukumar R, Yamakura T (2000) Science 288:1414
49. Craig AM, Banker G (1994) Annu Rev Neurosci 17:267
50. Giaume C, Koulakoff A, Roux L, Holcman D, Rouach N (2010) Nat Rev Neurosci 11:87
51. Kaech S, Banker G (2006) Nat Protoc 1:2406
52. Li Y, Yuan B, Ji H, Han D, Chen S, Tian F, Jiang X (2007) Angew Chem Int Ed Engl 46:1094
53. Chen ZL, Li Y, Liu WW, Zhang DZ, Zhao YY, Yuan B, Jiang XY (2009) Angew Chem Int Ed 48:8303
54. Jacobson BS, Branton D (1977) Science 195:302
55. Sun Y, Huang Z, Yang K, Liu W, Xie Y, Yuan B, Zhang W, Jiang X (2011) PLoS One 6:e28156
56. Peng YR, He S, Marie H, Zeng SY, Ma J, Tan ZJ, Lee SY, Malenka RC, Yu X (2009) Neuron 61:71
57. Koch C, Segev I (2000) Nat Neurosci 3:1171
58. London M, Hausser M (2005) Annu Rev Neurosci 28:503
59. Edgar D, Timpl R, Thoenen H (1984) EMBO J 3:1463
60. Ullian EM, Sapperstein SK, Christopherson KS, Barres BA (2001) Science 291:657